Southern 'annular modes' simulated by a climate model–patterns, mechanisms and uses

I. G. Watterson

CSIRO Atmospheric Research

Aspendale, Australia

revision submitted to special issue of J. Atmos. Sci.

20 November 2006

Abstract

Both high latitude (HLM) and low latitude (LLM) modes of variability of zonal wind in the Southern Hemisphere have been identified. Through an analysis of a simulation for 1871-2200 by the CSIRO Mark 3 climate model, the extent to which these might both be described as 'annular modes', based on their statistical patterns, physical mechanisms, and usefulness in climate study, is assessed. The modes are determined as EOF1 and EOF2 of vertically integrated zonal and monthly mean zonal wind, for 1871-1970. These match well those from ERA reanalysis data and also from the earlier Mark 2 model. The mode index time series relate to largely annular patterns of local wind and surface pressure anomalies (with HLM giving the familiar 'SAM'), and other simulated quantities. While modes calculated from 90° sectors are only moderately correlated (mostly in the polar region) for HLM, the link increases with time scale. There is little such relationship for LLM. A momentum equation analysis using daily data confirms that both zonal modes are driven by eddies, but only HLM features a positive eddy-mean flow feedback. Variation in feedback and surface damping through the seasonal cycle relate well to that in index autocorrelation, with the HLM being more persistent in summer. Stratospheric winds feature a long-lived component that tends to lead the HLM. The HLM drives sea surface temperature anomalies that persist for months, and coupling with the ocean increases variability on longer time scales. The annular variability in the warmer climate of the 22nd century is barely changed, but the mean climate change in the far south projects strongly on the HLM. The LLM features some statistical annularity and may have some uses. However, only the HLM can be considered to be a physically-based mode –the zonal wind equivalent to the one Southern Annular Mode.

1. Introduction

'What is meant by the words annular and mode?', asked Ambaum et al. (2001) (p3506), with respect to atmospheric variability. This is a fair question, since the words are hard to find in meteorological glossaries. A typical dictionary will offer 'ring-shaped' and 'most frequent value in a data set' (matching the meaning for mode given in the AMS Glossary). A geographical pattern of variability that features a zonal band does form a ring around the North or South Pole and is thus annular in shape. Leading patterns extracted through principal component (PC) analysis are perhaps modes in this statistical sense, and empirical orthogonal functions (EOFs) have commonly been referred to as modes.

Another meaning for mode exists in physics, being 'the pattern of motion of a vibrating body' (e.g., www.oxfordreference.com). In this context Ambaum et al. (2001) and Wallace (2000) argued that a fundamental mode of atmospheric variability should contain some imprint of a physical mechanism, in the present case involving a whole zone rather than just a sector. This could justify the name annular mode even for the Northern Hemisphere, where zonal asymmetry is substantial. Gerber and Vallis (2005) show that statistical annularity (to coin a phrase) in the structure of an EOF can occur without such a mechanism. Further, Cohen and Saito (2002) argued that the degree of annularity should depend on the relationships between different regional variations that contribute to an annular EOF. For the Southern Hemisphere (SH), the first EOF of geopotential height analyses (e.g., Kidson 1988b; Gong and Wang 1999) has a clearly annular pattern, at least. Furthermore, the EOF1 of surface pressure, commonly known as 'the southern annular mode' or SAM (Thompson and Wallace 2000), appears to be of considerable use in understanding the structure of climate change (e.g., Cai et al. 2003). Ultimately, a pattern most warrants a name if it useful!

Among earlier analyses of the SH variability, Kidson (1988a) highlighted the first two

EOFs of zonal mean 500 hPa zonal wind, and showed that these related to geographical patterns with an annular shape. Based on the latitude of their variability, these patterns have often been known as the high latitude mode (HLM) (e.g., Karoly 1990) and low latitude mode (LLM) (e.g., Cai and Watterson 2002). The aims of the present study are to compare these zonal wind EOFs, and to assess the justification for calling them annular modes, from a broad range of considerations. These include their statistical patterns and relationships, mechanisms and interactions, and, briefly, their uses in climate change. It is clear from more recent studies that the HLM of zonal wind is closely related to the SAM. But the question can be asked, is there more than one southern annular mode?

To further complicate the matter of names, various authors have characterised the leading modes in either hemisphere through their temporal character, as represented by an index or PC series. Zonal-index cycle was an early name, and oscillation has been popular, but both of these suggest variation within a limited frequency range. The actual daily series for the HLM varies more erratically, and was modeled as a stochastic process by Robinson (1994), Kidson and Watterson (1999) and others. It has been described as a vacillation by Yu and Hartmann (1993) and Watterson (2000).

Various physical mechanisms are of potential importance to an annular mode. Synoptic scale variability, storms or eddies, have long been recognised as the short-term driver of such modes, but individual storm events tend to occur within sectors of some 90 degrees longitude, and physical annularity is not assured. The modes themselves are not generally considered to be 'instability modes', although Frederiksen and Frederiksen (1993) suggest that barotropic instability may play a role for the HLM. In any case, wave-mean flow feedback has been shown to be important in enhancing its longer-term variability in both observational reanalysis data (Lorenz and Hartmann 2001) and climate models such as CSIRO Mark 2 (Watterson 2002). The length and self-consistency of data sets available

from model simulations supports their use in such analyses, particularly for the SH. The simplicity of the zonally and vertically-integrated angular momentum equation in interpreting the time variation of the modes (Feldstein and Lee 1998) encourages further use of zonal wind as the basic variable. The relationship of modes to variation in the zonal jets (an underlying theme of this volume), is readily seen.

While the focus here is on annular variability in the southern troposphere, the role of the stratosphere has long been of interest and is of potential importance to SAM on intraseasonal timescales, particularly in (austral) spring (e.g., Baldwin et al. 2003; Reichler et al. 2005). Likewise, anomalous fluxes of heat and stress at the surface associated with atmospheric modes can drive a substantial component of oceanic variability. This provided some feedback onto the atmosphere in the Mark 2 model (Watterson 2000), and the model of Sen Gupta and England (2006). In analyses of these potentially annular mechanisms, and of climate change, use of monthly mean data is convenient.

We can consider most of these aspects of annular variability in one paper by focusing on the new, enhanced-resolution, CSIRO Mark 3 (or Mk3) climate model (Gordon et al. 2002), and using approaches applied to Mark 2 in previous studies. Basic descriptions of Mk3, the simulations, and the data sets used are given in the following section. Principal component analysis is applied to both 6-hourly and monthly-mean SH winds in section 3 and the two main modes are described. Some comparison will be made to reanalysis data, to demonstrate the validity of the model. Seasonal variation of the patterns and relationships to other variables will be shown. Section 4 considers the spatial coherence of patterns, including results from four 90° sectors, in the context of the test for annularity proposed by Cohen and Saito (2002). Section 5 considers the evolution of the annular structures, and its variation through the annual cycle, in some depth. Interactions with the stratosphere and the ocean are briefly considered in section 6. Finally, some basic

results from an analysis of climate simulated by Mk3 for the 22nd century are given in section 7.

Some discussion and conclusions regarding the annularity of both HLM and LLM are included in the sections. An overall summary is given in section 8, and an assessment made of the merit of the term 'annular mode' applied to both the simulated southern wind patterns.

2. Simulations by Mk3

a. Model

The CSIRO Mk3 coupled atmosphere-ocean model is a substantial upgrade to Mk2, fully described by Gordon et al. (2002). With regard to atmospheric variability, the most notable change is in resolution. The horizontal resolution is T63 (defined spectrally) or around 1.8° of longitude (and latitude) compared to R21 or 5.6° for Mk2. Vertically, there are two levels for each of Mk2's nine sigma levels, with $\sigma = p/p_s$, where p is pressure, and the subscript 's' denotes surface. A hybrid (σ:p) coordinate is now used, with the denominator being a weighted average of p_s and 1000 hPa. As is typical of a climate model, the layers are spaced symmetrically about the middle coordinate value 0.5, with five above 0.2 in Mk3. The levels are close to sigma near the surface, and isobaric towards the top-of-atmosphere (defined as 0 hPa), with the top level being 4 hPa. With the focus being the troposphere we will continue to describe the levels or corresponding layers as being in sigma, for convenience.

Like Mk2, the Mk3 ocean is based on the GFDL MOM code. It has two grid boxes for each atmospheric grid square (from halved latitude spacing), and 31 levels, with the upper three layer thicknesses being 10, 12, and 14 m.

A now-standard set of physical processes are modeled, including the land surface, dy-

namical sea ice, cloud formation, precipitation, convection, and radiation. The radiation in the model is perturbed through variations in the specified ozone distribution and greenhouse gas (GHG) concentration. Some effects of anthropogenic aerosol are included through a surface albedo adjustment.

b. Simulation and data sets

The simulation of the model that is analysed here is one of an ensemble contributed to the 'IPCC model output' data set (available from www-pcmdi.llnl.gov). It represents climate over the years 1871-2200, with observationally-based 'forcing' for the years to 2000 (as described by Watterson and Dix 2005). Forcing in the 21st century follows the 'A1B' scenario, which by 2100 has an effective GHG concentration some three times the 1871 value, but an ozone distribution restored to the original (in Mk3). The concentrations are stabilized from 2100 on.

While some analysis of the intervening years has been done, the focus here is on the first and last centuries. Two main data sets have been used in the analysis of 1871-1970, loosely denoted '20C'. The first is of basic atmospheric fields, including zonal wind u and meridional wind v from all sigma levels and the full horizontal grid saved 6-hourly. The second is of monthly means of most simulated quantities. As for Mk2, atmospheric data are interpolated to the (18) pressure levels corresponding to the sigma values times 1000 hPa. For convenience we denote the two sets, and the corresponding analyses, by daily and monthly.

c. SH means and variability

The climatology (time mean) for the 20C period is generally similar to that presented in the previous Mk3 studies, and the model is among the more realistic coupled atmosphere-ocean models in reproducing the observed SH climate.

The basic variable for the PC analysis is the focus here. The monthly mean zonal winds have been vertically integrated from the surface (allowing for topography) to the top-of-atmosphere, with respect to pressure (hence with mass weighting). This produces a quantity proportional to momentum, but to retain the dimensions of wind, we can divide the result by 1000 hPa and denote it U. Away from the equator, the zonal mean of U is typical of mid-tropospheric winds. The full-year means of zonal mean U over southern latitudes are shown in Fig. 1. The model winds closely match the 'ERA' reanalysis result also shown, including both a jet peak around 50°S and an extended northern flank. The data used are from the whole years 1958-2001 from the ERA40 project described by Kållberg et al. (2004), including levels through 30 hPa. Within the troposphere, biases are mostly within $2\,\mathrm{m\,s^{-1}}$, as the midlatitude bias in Fig. 1 is enhanced by a westerly bias in the model stratosphere. There is rather little variation in the strength of the model jet peak through the mean annual cycle, as seen from Fig. 2a. The increase in late winter is actually due to stratospheric winds. However, the latitude of the peak varies (Fig. 2b), being poleward in March as in the observations (Codron 2005), and again in spring (although this shift is greater in ERA). In the poleward months there is a distinct upper tropospheric jet peak at lower latitudes. These winds peak in winter, as evident from U at 36°S shown in Fig. 2a.

To remove externally forced variation, the mean winds are removed at each latitude, for each of the twelve months in turn, so leaving anomalies relative to the mean annual cycle. Likewise any linear trend over time is removed. Finally, the variability in zonal means

forced from the tropics by ENSO (Seager et al. 2003) is removed using linear regression, again for each month separately. For observations, the ENSO index is defined by the NINO3.4 series: anomalies of sea surface temperature (SST) averaged over 5°S to 5°N and 170°W to 120°W. In the case of Mk3, Watterson and Syktus (2006) find that the model ENSO is better defined by SSTs further west (150°E to 190°E). In both Mk3 and ERA the ENSO index correlates with low-latitude U, with the coefficient r reaching values of 0.5 (not shown) between monthly means. This positive band extends to about 50°S in summer, while further south r varies between about ± 0.2. It should be noted that $r = 0.2$ is statistically significant only at the 5% level, for a sample of 100, and not significant for the 44-point ERA record. However, this level is reached at $r = 0.06$ for the 1200-month series, and $r = 0.09$ in the monthly ERA case. These values can serve as an indication of the confidence we can have in later r results.

The final monthly U anomalies have a standard deviation (SD) as a function of latitude, also shown in Fig. 1. The model produces an accurate match of the ERA result, with clear peaks in variability around 60°S and 40°S, on the flanks of the main jet. This appears consistent with variation in the latitude of the jet. The low latitude variability has a weak minimum in the vicinity of the subtropical jet, also suggestive of variability of the jet position.

3. Principal components

a. Monthly

We consider initially modes defined using data from all months. Principal components of the monthly U anomalies are determined using the NAG routine g03aaf (see www.nag.com). Weighting by area is included, and the results normalized so that each PC series has zero

mean and a SD of 1. The EOFs then give the wind anomalies for an PC value of one. In ERA the first mode has 46% of the variance and the classical HLM structure (Kidson 1988a). This is shown in Fig. 3, with the sign of the EOF chosen so that the poleward lobe is positive. In Mk3 the EOF1 has a slightly greater fraction (53%) but the structure is very similar.

The second modes (20% for ERA, 22% for Mk3) are also very similar to each other. This structure is clearly the LLM, with wind peaks around 47°S and 27°S. Given that EOF2 is defined to be orthogonal to EOF1 (e.g., Ambaum et al. 2001), it is not surprising that the southern latitude is close to the node (zero) of the first. Nevertheless, the LLM does appear to relate to the subtropical jet. Its subtropical lobe overlaps latitudes strongly influenced by ENSO, hence the importance of removing that component. The higher EOFs contain considerably less variance and have multiple lobes, and appear to be of little interest here.

Some seasonal variation in these modes can be anticipated, given that in the jet. Partitioning the Mk3 PC series by month of the year results in series of 100 values, still with zero mean, but a SD that need not be unity. These SDs are plotted in Fig. 2a, with a scale factor proportional to a representative wind speed of the mode (w, given in Table 1) determined by taking the square root of the hemispheric mean variance of the EOF. The SD of PC2 peaks in July, with a ratio 1.79 to that in January. The variation follows fairly closely the variation in the mean U at the EOF2 node (36°S). The variation in PC1 is somewhat smaller (ratio 1.48) and has little relation to that in the main jet peak speed, or the small variation in speed at the node latitude. A seasonal shift in the position of the HLM can be deduced, however. Regressing the entire PC1 (x) against the U anomalies (y) reproduces the EOF1 as the regression coefficient b (in the linear regression equation $y = a + bx + \varepsilon$). Performed with partition by month, regression produces a node that varies as shown in Fig. 2b (Reg). Given this, it is worth comparing with results from EOF anal-

ysis performed individually for each month. The resulting nodes (Ind) are similar. This is because the new PCs are highly correlated with the partitioned values. A mild exception is for July, when r falls to 0.87. For simplicity, it is sufficient to rely on regression using the all-month PC series to reveal seasonal variation of the modes. These series will be referred to as the HLM and LLM (monthly) indices.

b. Daily

The sigma level zonal wind data from Mk3 have been vertically integrated and scaled as above, to produce zonal mean winds at each latitude and 6-hourly time step. The ENSO component is removed on a monthly basis, as before, and anomalies relative to the full annual cycle formed. Naturally, the resulting quantity has more variance than the monthly means. The first mode (41%) from this data set is very similar in structure (Fig. 3) to the monthly EOF1, with w 40% larger. The second mode has a primary node slightly to the south, and also features an exaggerated high latitude component. This picks up some of the daily variance on the far southern flank of the main jet, allowing PC2 to explain 23% of the total variance and w to be 59% larger. In fact, regression partitioned by month shows that this southern component mostly occurs during autumn, when the main jet peak is furthest south. It is worth noting that the structure of the daily LLM means that it is closely related to the zonal mean of a standard blocking index (Pook et al. 2006).

Forming monthly means of the daily PC1 virtually reproduces the monthly PC1 ($r = 0.9999$) aside from an amplitude factor, while the correlation between the corresponding PC2 series is nearly as close ($r = 0.987$). The seasonal variation of these indices differs somewhat, nevertheless. The SD of the HLM daily index partitioned by month is more uniform (than Fig. 2a), being relatively larger in autumn and smaller in spring, for reasons

explored in section 5.

c. Relationships

Returning to the monthly mean data, the regression between the indices from all months and zonal mean U produces correlations over 0.9 at the EOF1 lobe peaks, so that nearly all the variance there is associated with the HLM. (Note that r and b are simply related: $r = b\sigma_x/\sigma_y$, where σ denotes SD, using the series from 3a.) Even with the ENSO component of U included (as in all these regression results) the correlations for EOF2 reach 0.8 at 27°S. Large r occurs for the zonal means of u at individual tropospheric levels also. The dimensional regression b results for both HLM and LLM are shown in Fig. 4. The peak winds occur in the upper troposphere where variability is larger. Anomalies extend into the lower stratosphere also, particularly around 60°S and in summer.

Strong relationships with the modes occur for other atmospheric variables at certain latitudes and pressures. The meridional wind v anomalies peak near the surface, as shown for HLM in Fig. 4c. Divergence near the node latitude is matched by convergence aloft. Midtropospheric temperatures (T) are higher above the node, and lower on the flanks (similar to results for Mk2 shown in Watterson 2000). The LLM results are comparable in structure, but shifted north and typically weaker.

Correlations with local anomalies are, naturally, smaller than those with zonal means, but they can still be important. Values between HLM and U reach 0.6 over the Southern Ocean, as seen in Fig. 5. Correlations for LLM are smaller, particularly in the subtropical lobe. While both lobes are evident at virtually all longitudes, the largest r for both modes occur around 180°E. Similar patterns, but with somewhat larger r, hold for correlations between annual mean anomalies, confirming that the modes relate to interannual and longer period variability (Watterson 2001).

Some zonal asymmetry is seen in the observed SAM sea-level pressure pattern (e.g., Sen Gupta and England 2006). The Mk3 regression result for the HLM, shown in Fig. 6a, is quite similar to SAM in the location of its peaks, and in having weaker midlatitude anomalies in the far eastern Pacific. All the polar region is negative, allowing a meridional gradient that supports, by geostrophy, the westerly anomalies at all longitudes (Fig. 5a). While the zero contour encircles the high latitudes for LLM (Fig. 6b), the anomalies are weak and asymmetric near the pole. An important quantity with regard to the ocean, and which illustrates the near-surface wind direction, is the surface stress vector field, also shown. Again, this contains some zonal asymmetry, particularly for LLM. Associated with the zonal mean pressure changes is a net meridional shift in atmospheric mass, out of the polar region in the case of increasing HLM. This is directly associated through geostrophy with only part of the U change, given the relatively small low-level winds (Fig. 4). Naturally, all these anomalies occur with the opposite sign also, and like those for U have some seasonal variation.

Associated with the low-level divergence/convergence and surface pressure anomalies are substantial anomalies in precipitation at some latitudes. In monthly means, the correlations between the indices and zonal mean precipitation exceed 0.7 for HLM , and 0.6 for LLM. Correlations at grid squares can also be significant, including at some locations in South America and Australia. Surface temperature, of both land and ocean, is also affected. The model results for HLM compare very well with the relationships between station data and SAM presented by Gillett et al. (2006). This supports the use of the HLM, at least, in interpreting climate change. Given our present purpose, discussion of the ocean temperatures is deferred to section 7, while precipitation will be considered in another paper.

Before leaving this section it is worth confirming that similar indices can also be ob-

tained using principal components of these related dynamical quantities. Truncating the vertical integral of monthly u at about 125 hPa (by omitting data levels 15-18) virtually reproduces the HLM and LLM indices. This will be considered again in section 6a. Using zonal mean SLP produces a PC1 correlating with the U HLM index with $r = 0.88$, and an EOF1 similar to the zonal means of Fig. 6a (and shown later). For the second modes r falls to 0.69.

Overall, it seems that in Mk3 the HLM index is almost independent of the method of definition, but the LLM index is less well defined. The zonal wind HLM is closely related to the SAM pressure pattern. Nevertheless, the LLM represents a substantial fraction of midlatitude variability at most longitudes, and is in a limited statistical sense rather annular.

4. Variability within sectors

Even with zonal symmetry of anomalies, the question can still be asked whether the EOFs of U represent an inherently annular component of variability. Cohen and Saito (2002) found that the degree of annularity varies among cases, depending, in essence, on the ratio of variance that is common to all longitudes to variance confined to regions. We explore here a simple partition of the hemispheric data into 90° sectors, with the first sector ('S1') starting at 0°E. Conveniently, with regard to climate, three sectors contain a continent in the midlatitudes, with Australia centered in S2.

Taking zonal and monthly means of U within each sector and performing PC analysis produces dominant modes that resemble the zonal-mean HLM and LLM, and can be categorized under the same names. The nodes occur at latitudes at most 2.1° from those of the two zonal-mean cases in Fig. 3. The amplitudes of the sector EOFs are somewhat larger, particularly in the equatorward lobe, but with some variation. The representative

wind speeds (w), given in Table 1, indicate that the HLM in S3 is in fact EOF2 (with less variance than LLM in S3). Each sector HLM index is moderately well correlated with the zonal HLM index (Table 1), but less well for LLM. Cross correlations between sectors (Table 1) are modest, averaging $r = 0.40$. Interestingly, they all increase for annual means of the indices, with the average rising to $r = 0.63$. For LLM they are quite uncorrelated, except for S2 and its neighbors, and with little change on annual averaging.

A corresponding analysis using the daily data produces modes with similar structures, but wind speeds up to double the monthly sector values. There is less variation in w between the sectors in the daily case. Now, projecting an EOF on the U anomalies reproduces the associated PC series. Since the zonal anomalies are the average of the sector anomalies, the similarity in mode structures means that the average of the four sector indices is very well correlated with the zonal index, for both HLM and LLM. In fact, if each sector index is first multiplied by the ratio of its w to the zonal mode w, the zonal series is closely reproduced. The average value of this ratio is shown as the lag-0 regression values for the pair S-S in Fig. 7.

The correlations between the zonal and sector HLM daily indices are between 0.51 and 0.63, a little lower than for the monthly case. The cross correlations are relatively small, at zero lag, reaching $r = 0.29$ for the HLM S2 and S3 pair. This pair is likely favored because they share anomalies occurring in a band of variance around 180°E. Shown as regression coefficients in Fig. 7, the lag-0 relationship for HLM is typically weaker for opposite sectors (across the pole) than for adjacent sectors ('e' or 'w'), but still positive. For LLM the average is near zero for each case.

In theory, averaging four independent sector index series of the same SD produces a zonal index with SD halved, and which correlates with each sector index at $r = 0.5$. The daily LLM results are rather consistent with this. Interdependence of the sectors is greater

for HLM and the sector w values smaller relative to the zonal w (as seen in Fig. 7, lag 0). There appears to be some common, zonal, component of variability in HLM, and hence some degree of annularity in this sense. Furthermore, this annuality increases with averaging time. There is little such annularity evident in the LLM case. The specific test for annularity used by Cohen and Saito (2002) considered a partition into only two sectors. Simply adding pairs of our sector monthly indices, and removing each result in turn from the zonal index by regression allows a comparable test. This also supports some annularity for HLM and little or none for LLM (depending on the criterion for r used).

Relationships between the sector indices and quantities at grid points within the sector can be large, such as for the monthly means and S2 HLM in Fig. 6c. However, even for this strongest sector HLM, the equatorward lobe and midlatitude SLP have very small amplitude outside the sector. The poleward anomalies still encircle Antarctica, however. Correlations between daily indices and SLP (not shown) are largely confined to the sector, although for HLM there is still some coherence around Antarctica. Further insights are gained from consideration of the temporal evolution of the patterns in the next section.

5. Evolution of modes

a. Correlations between time-lagged indices

A simple statistic for persistence of the indices is the lagged autocorrelation. For the monthly indices, at lag 1 month, this is $r = 0.42$ for HLM and 0.29 for LLM. A spectral analysis of each time series produces no prominent peaks, and each spectrum lies within the range expected of a simple Markov process on a one-month timestep with these values (as for Mk2, Watterson 2001).

The monthly r values are larger than the 30 d lag values for daily indices, due to some

filtering of short-term variation by the monthly averaging. The autocorrelation of the daily indices falls, most rapidly in the first week, to 0.19 for HLM and 0.07 for LLM at lag 30 d. This fall is illustrated in Fig. 7 (the Z-Z case).

The various sector indices have lower persistence, in terms of r, than the zonal indices. For the monthly cases r at lag 1 month ranges from 0.25 to 0.30 for HLM and 0.13 to 0.21 for LLM. Interestingly, the cross-correlations at lag ± 1 month for HLM are nearly as large averaging 0.22, while those for LLM average only 0.07. It is revealing to examine the related daily regression results in Fig. 7. For both HLM and LLM the index for the sector to the east (the S-S_e case) increases over the following week (the bump at lag 2 d for HLM is due to the pair S2 and S3). The large rise for LLM seems to be at the expense of the first sector, whose index (from S-S) falls below that to the east. A similar effect (for SAM) is evident in the new studies of Gerber and Vallis (2007) and Codron (2007), associated with regional anomalies that tend to propagate to the east.

The fall in the first week of the sector to the west mirrors the earlier rise of that to the east (and other results are essentially symmetric with lag, justifying the restricted negative range in Fig. 7). The opposite sector HLM continues to increase through a second week suggestive of further propagation eastwards. By day 20, the four S values shown are similar and persisting; the other three sectors are as anomalous as the first. Gerber and Vallis (2007) show an equivalent result, and argue that this is evidence of a physical mechanism supporting annularity. Such evidence is lacking in our LLM case. The sector opposite is essentially unrelated to the first at all lags. These results can be related to the surface pressure patterns in Fig. 6. Even in the HLM sector case (6c), pressure is low throughout a zonally symmetric polar region, and the geostrophic wind projects on each sector EOF. This does not occur for the LLM, which is apparently too far from the pole.

Returning to the zonal-mean case, there is more persistence of the HLM in summer,

using the daily indices partitioned by month, as shown in Fig. 8. In terms of an e-folding time, the values range from 28 d in January to 11 d in April. A similar variation in e-folding time is evident in tropospheric data analysed by Baldwin et al. (2003), except that the Mk3 peaks are a month or so later. The variation in r for the monthly indices is between 0.52 and 0.24, peaking in the same months as in Fig. 8. In contrast, LLM is a little more persistent in winter, with monthly r peaking at 0.40 in June, when the HLM value is 0.42.

To better understand this temporal behavior, and the seasonal variations, we turn to the dynamical equations.

b. Zonal wind equation

Following previous authors (in particular, Watterson 2002) we consider the equation for zonal mean zonal wind at each sigma level in the simplified form

$$\bar{u}_t = f\bar{v} + F_E + F_M + D, \tag{1}$$

where an overbar denotes the zonal mean and a prime the zonal anomaly, v is the meridional wind, f the Coriolis parameter, and the t subscript indicates the time partial derivative. The terms $F_E = -(a\cos^2\phi)^{-1}\partial(\overline{v'u'}\cos^2\phi)/\partial\phi$, and $F_M = -(a\cos^2\phi)^{-1}\partial(\bar{v}\bar{u}\cos^2\phi)/\partial\phi$, are the eddy and zonal mean flux convergences respectively, with a the earth radius. D is calculated as a residual. For each of these functions of latitude, we can project the (daily) EOF for each of HLM and LLM onto the detrended anomalies relative to the 100-y annual cycle, to produce a 6-hourly time series. (Projection reduces the unit to s^{-1}, but we retain the names of the terms.) The vertical integral of the term on the left side ($\bar{u}_t$) closely reproduces the derivative of the PC series or index. Regressing the terms with lag against the index shows which terms contribute, on average, to the growth and decay of the index.

The vertical structure of the lagged regression b for terms in Eq. 1 in the HLM case is shown in Fig. 9. The $\bar{u}_t$ term is almost coherent vertically in lag time, with $\bar{u}$ peaking in the upper levels at most 12 hr after the peak at lower levels. The main driving term (at negative lags) is F_E. In the upper troposphere it is partially offset by $f\bar{v}$. That term is very large near the surface, where it offsets a similar but negative D term dominated by the first three or four sigma levels, and hence the boundary layer. As a residual, the D term also includes vertical advection terms (including eddy terms) that do not contribute to the vertical integral, as well as parameterized diffusion and drag in the model, but these appear relatively small aloft. The F_M term (not shown) is small. The terms have a similar broad structure to the Mk2 results (Watterson 2002), but at double the resolution.

The regression of the vertical integral of all the terms is shown for HLM in Fig. 10a. The $f\bar{v}$ term becomes small, but is non-zero. The net meridional movement of air leads to a pattern of $\bar{v}$ that makes a small projection on the EOF, which changes sign as the shift reverses at lag 0. The growth of the index is dominated by the eddy forcing term F_E, countered by D. Taking the ratio of the regression b results for the index ($\bar{u}$ here) and D produces an effective damping time scale. This is 8.6 d at lag 0, and only a little longer (up to 10%) at other lags. The near linearity of damping (except for short-term 'noise') is confirmed by a correlation coefficient between monthly means of the two terms of –0.95.

Variation in the terms of the zonal wind equation through the annual cycle can be seen by regressing data that is partitioned by month of the year. This shows that the damping strength (or inverse time scale) is seasonally dependent, as seen in Fig. 8. That the variation in the D residual is dominated by surface stress is supported by an almost identical variation (not shown) for b with respect to the zonal surface stress anomaly (projected on EOF1). In fact, r between the full series of stress and D is –0.99. What determines the strength of the damping is not clear from this analysis. Presumably, damping can vary

with the character of the boundary layer, and it is notable that the (level) D term extends to the fourth sigma level (0.9) only in the cooler months. The stress closely relates to low-level wind, so that part of the seasonal variation in damping time may relate to that in the vertical structure of the wind anomalies. The b for u at 946 hPa is in fact a little smaller in summer, consistent with wind anomalies associated with U reaching to higher, stratospheric, altitudes in summer.

The eddy forcing term also contains some variation with season, which will influence the amplitude of the mode (Fig. 2a). Partitioning the 6-hourly F_E series by month, and taking the SD, results in the variation shown in Fig. 8. This is rather like that in D, and typically smaller in summer. The final result shown in Fig. 8 relates to the feedback of the wind anomalies on the eddy forcing, i.e., a dependence of the forcing on u anomalies in previous days. This is seen as a component of F_E that persists in the lag-regression analysis beyond the index peak (excepting that due to the inherent life-time of the eddies themselves). It appears that after a short period of negative feedback, there is a positive feedback that acts for at least a month –indeed as long as the U anomalies.

For Mk2 (Watterson 2002), and for reanalysis data (Lorenz and Hartmann 2001), the positive feedback can be attributed to synoptic scale and short-lived eddies. The negative component results from larger scale waves, initially (around lag 2 d) in association with short-lived eddies (the 'cross-frequency' term). An analysis of 10 years of data from Mk3 produced similar results. While those studies developed a simple stochastic model for the HLM index, incorporating the feedback, for the present purpose we can simply assess it by averaging the F_E b in Fig 10a over the lags 10 to 30 d. This gives 0.018 per day for HLM. Partitioning the regression by the month of the index produces the variation shown in Fig. 8. The low feedback months partly coincide with a poleward position of the jet (Fig. 2b), as noted by Codron (2005).

There is likely some statistical uncertainty in the variation in the terms in monthly partitions, particularly of the feedback. Nevertheless, the net effect of damping and feedback qualitatively explains the variation in the persistence, with strong damping and low feedback in April–May, and the reverse in December–January.

Turning to the LLM, the lag-height structures of the terms are rather similar to those in Fig. 9, and for the vertical integral, shown in Fig. 10b, the forcing and damping roles match those of HLM. An important difference occurs at positive lags. The initial negative eddy feedback is stronger, providing a rapid reduction of the index peak, on top of that due to D. The subsequent positive feedback is weaker. The 10-30 d average of F_E in the vertical integral is 0.004 per day, much smaller than for HLM. This will also lead to reduced persistence for LLM. Lorenz and Hartmann (2001) made a similar comparison of zonal wind EOF1 and EOF2 in reanalysis data.

The simple zonal wind equation used above is not applicable to sectors, and an assessment of the role of various terms in driving the inter-sector relationships depicted in Fig. 7 is not attempted. Cash et al. (2005) and Codron (2007) explore the way anomalies in one sector can influence eddies in another, providing a dynamical mechanism supporting annularity. Presumably, the polar coherence of SLP anomalies associated with the HLM also plays a role. Simple propagation of wind anomalies from one sector to that to the east, which occurs for LLM (Fig. 7b), is evidently not sufficient to produce a positive feedback.

It is worth pointing out, with regard to some earlier studies, that the simple time-filtering of monthly averaging produces an F_E series that is well correlated with the monthly index: 0.82 for HLM and 0.71 for LLM. This is largely a result of the driving role of F_E (during the negative lags in Fig. 10). It need not relate to the feedback, which is evidently near-zero for LLM in the annual case.

From Fig. 10b, the mean damping timescale (9.4 d at lag 0) for LLM is actually a little longer than that for HLM. The statistics used in Fig. 8 show a larger seasonal variation for LLM, with damping strength in late winter double that in summer, rather consistent with variation in the associated low level wind (and the vertical structure). Countering this is a moderately positive eddy feedback in early winter, which contrasts with a weakly negative feedback in summer. This, and larger forcing in winter, appear to relate to the variations of the jet (e.g., Fig. 2a). It is evident that in winter the Mk3 LLM behaves rather like HLM in this respect, while in other seasons it is weaker and less persistent.

c. Meridional propagation

So far we have focused on the variation in time of the HLM and LLM indices, since these act as amplitude factors. While this is reasonable for the large variations within a month, there can also be changes in meridional structure during the evolution of the modes. It is convenient to depict this using monthly means. Regressing the indices with zonal means of U, lagged over one or more months, produces the b coefficients shown in Fig. 11. At lag 0 the pattern is essentially the EOF. At lags ± 1 month the values at the peak latitudes drop roughly in accordance with the index autocorrelation. However, there is also an apparent meridional propagation of the pattern. This is fast enough in the subtropics to allow a weak positive peak at lag 1, in the HLM case. While the magnitudes of these winds are small at lags ± 2 months in this annual case, for HLM they are greater in the more persistent summer months (not shown), when the node clearly moves southward some 10° over four months.

The LLM subtropical lobe appears to propagate in from the tropics (Fig. 11b), while the midlatitude node moves some 5° per month. Such propagation can curtail the persistence of the LLM index, even if anomalies remain. The role of eddies in such propagation has been

considered by Lorenz and Hartmann (2001) and others. Presumably, the eddy feedbacks on the LLM index differ from those on HLM in part because of the faster propagation. The shift in the EOF2 pattern also means that, although the HLM and LLM indices are uncorrelated at lag 0, the r at lag (Table 2) are non-zero. The HLM can be said to lag the LLM, although rather weakly.

Summarizing this section, in Mk3 both HLM and LLM are driven by the convergence of eddy momentum flux. Both are damped through boundary layer friction, aided by a short-term negative eddy feedback that is particularly strong in LLM. A positive eddy feedback boosts the persistence of the HLM during most of the year, in contrast to LLM. While individual sectors vary rather independently from day to day, their variability persists in an annular fashion in HLM, while in LLM there is only some eastward propagation of anomalies. This points to a weak but truly annular mechanism on the weekly to monthly timescale for HLM, but not LLM.

6. Interactions

Interactions between the troposphere and the layers above or below have the potential to support additional mechanisms that enhance the HLM or LLM.

a. Stratosphere

It was noted in 3c that excluding the stratospheric data levels ($p < 125$ hPa) in the vertical integral of u, to produce the 'tropospheric' wind 'Utr' had little effect on the resulting monthly HLM and LLM indices. In fact, the representative wind speeds of these EOFs are slightly higher that those in Table 1. This is true also of the ERA40 results (c.f., Feldstein 1998), and the correlations between the pairs are also high (0.99 for EOF1, 0.95

for EOF2). Still, the small numerical effect of including the stratosphere may not reflect its actual effect on the evolution of the modes. While Mk3 does not have the resolution to fully model stratospheric dynamics, it is of interest to briefly consider here whether the stratosphere relates to the two simulated SH modes in similar ways.

We focus on zonal mean u at 54 hPa, which from Fig. 4 has some relationship with both HLM and LLM. Following Baldwin et al. (2003) we calculate the EOFs of this field, and denote these u50-1 and u50-2. These have structures resembling the HLM and (less so) the LLM, as can be seen from the lag-0 regression results in Fig. 12. The representative winds of these modes are still similar to those for U in Table 1. A similar calculation for 50 hPa wind from ERA40 produces an EOF1 describing tropical variability, which the model lacks. EOF2 is the HLM, although it is more focused on 60–65°S than that in the troposphere.

The new model indices have greater persistence than the U ones, with r at lag 1 month of 0.57 and 0.61, respectively. The winds in Fig. 12 show this, and also a shift poleward over several months. The ERA40 stratospheric HLM has a similar overall persistence of 0.54. While there is some seasonal variation in the model HLM (with persistence reaching 0.7 in winter), this is not as large as in the observational case, which has a sharp peak in both amplitude and persistence around November. Unlike the model, this coincides with enhanced persistence in the troposphere. We focus on the usual, and more statistically certain, full year results from the model.

The correlations between the u-50 and U indices are given in Table 2. At lag 0, these are only moderate. Interestingly, there is a lop-sided lagged correlation for the HLM pair. This is consistent with the spatial evolution of u50-1, with the wind at lag 1 having a greater projection on HLM than at lag –1.

Consider then the relationship between u-50 and the Utr winds, which are potentially

unrelated. Again the tropospheric Utr-1 tends to lag u50-1. This is not seen for the second modes. To clarify this, one can remove the component of u50-1 that is 'independent' of Utr-1 (using the regression b). The progression of r with lag is again given in Table 2. The regression between this 'u50-1i' index and the Utr winds at all latitudes is shown in Fig. 13. The propagation southward of the anomalies is clear. At lag-0 the anomalies project on the tropospheric LLM, as quantified by r in the third last line of Table 2.

Regressing the u50-1i index against the monthly means of the terms in Eq. 1, projected on the HLM (as in Section 4b), confirms that the HLM tends to grow (albeit weakly) when u50-1i is positive. Furthermore the F_E term appears to drive much of this growth, as in a comparable analysis of the observed NAM by Baldwin et al. (2003). However, an alternative view of the SH evolution in Mk3 is that the tropospheric LLM anomalies contribute to u50-1. As the LLM propagates southward, the HLM is also perturbed. This mechanism would resemble to some extent that proposed by Reichler et al. (2005), except that the importance of the model stratosphere is unclear. There is greater potential for the stratosphere to contribute in reality, particularly in spring.

With respect to the present aim, the analysis demonstrates that the model stratosphere contributes a low-frequency component to both the HLM and LLM. However, it is not, numerically at least, large enough to significantly modify either mode. The stratosphere does not appear to have a direct role in explaining the seasonal variation in the persistence of the tropospheric modes in Mk3.

b. Ocean

As noted in section 3c, ocean surface temperatures in Mk3 are perturbed by the HLM, and to a lesser extent the LLM. This process was previously examined in depth for Mk2, and limited analysis here suggests that surface heat fluxes play a similar role in driving

the anomalies in Mk3. Much of the pattern reflects the near-surface wind speed anomalies that directly affect evaporation. Over ocean these fluxes are aided by surface stresses (Fig. 6) and the associated oceanic currents and overturnings. The high latitude temperature relationship with HLM, under the region of lower SLP, is mostly negative, except for a warmer region around the Antarctic Peninsula. Sen Gupta and England (2006) analyse a similar simulated pattern in depth. In maps of the correlations with annual mean SSTs (not shown) only HLM has substantial anomalies extending around zonal bands.

With regard to a potential two-way interaction between the modes and the ocean, it is revealing to consider the regression b for zonal and monthly mean ocean surface temperature with lag, shown for HLM in Fig. 14a. The midlatitude SST peaks occur at lag 1 month, and then persist for several months, at least. While the magnitudes are small, they represent correlations up to 0.6. The larger (but with smaller r) anomalies near the Antarctic coast are for averages over much shorter zonal distances, often over sea ice, which has a thin surface layer. The SST anomalies are similar to those in Mk2 (Fig. 10 of Watterson 2000), except for a smaller subtropical component. A response of the SSTs to LLM also occurs (Fig. 14b), but at equatorward latitudes and with short-lived anomalies at most half as large, consistent with the smaller winds.

A small, annular, influence of the mid and low latitude SST anomalies associated with HLM back on the atmosphere was detected in Mk2 (Watterson 2000), but this did not match the HLM itself. Rather, the wind response tended to move the mode polewards as it decayed. In any case, variability and persistence of the index were enhanced by the interactive ocean (Watterson 2001).

To test these effects in Mk3, two 54-yr integrations with an uncoupled atmospheric version of the model, with SSTs specified to follow observations over 1949-2002 (Watterson and Syktus 2006), have been analysed, including removal of the ENSO component. These

show similar poleward propagation of U to Fig. 11 for both HLM and LLM, however, suggesting a role for eddies in Mk3 rather than ocean feedback in causing the propagation. A small increase in persistence of the monthly indices due to the ocean occurs in Mk3, with r at lag 1 month in the uncoupled runs averaging 0.30 for HLM (compared to 0.42 for the coupled case -section 5a), and 0.24 for LLM (0.29).

The greater persistence of the modes in the coupled Mk3 is reflected in the variability of annual means formed from the monthly indices. For HLM the ratio of the SD of the annual means to that of the monthly series (SD unity) is 0.43, while for LLM it is 0.35. For the uncoupled runs the ratios fall to 0.38 (HLM) and 0.31 (LLM). Thus HLM becomes more dominant at interannual periods, and is amplified by coupling. However, there is no spectral peak out to decadal time scales in these indices. It is worth noting, though, that the variance of LLM is considerably enhanced if the projection of ENSO on it is included. In fact, in the coupled Mk3, the annual mean series for this enhanced LLM has SD 0.43, while the HLM SD is barely changed at 0.44.

In summary, while there is an important near-annular impact of the HLM on the ocean, the results do not support the interpretation of either mode as truly 'coupled', with respect to the ocean, on the sub-decadal timescale. The ocean-interaction mechanism provides only weak support for true annularity of the HLM, and none for LLM.

7. Climate change

As the final topic in our examination of the two SH zonal wind modes, we consider briefly the climate change simulated by Mk3 under the A1B scenario. Miller et al. (2006) show that the simulation for the same scenario by other climate models produced a trend in SLP to 2100 that projected positively on the SAM pattern, as the global temperature rose. In a comparable scenario, Cai et al. (2003) showed a similar trend to 2100 in Mk2. Continuing

beyond this with constant GHG, the simulated warming rate slowed, while the projection on SAM diminished.

Our focus here is the difference between the two 100-y periods, the original period 20C and the years 2101–2200, or 22C. This relates to a global mean warming (in T_s) of 2.7 K. This slightly underestimates the forced response of the model because of a slow cooling trend in an unforced or control simulation (Watterson and Dix 2005). The warming trend over 22C is 0.3 K per 100 y (again, an underestimate).

The latitudinal distribution of the warming in the SH is shown in Fig. 15a. In the annual result there is a minimum in warming in the Southern Ocean, although this varies seasonally (in part due to effects of sea ice). The changes in SLP are shown in Fig. 15b. For each season, the pressure decreases near the pole and increases in the mid latitudes. This does indeed project on the EOF1 of zonal mean SLP anomalies, determined from 20C (see section 3c). In fact, in terms of PC1 the value for the annual change is very close to one, see Table 3. This 1×SAM pattern matches the polar change but underestimates the SLP change in the mid and low latitudes. The change projects negatively on the EOF2 of SLP. A combination of the two modes can match the pressure change well to about 45°S.

The change in vertically integrated zonal wind U is given in Fig. 15c. The high latitude winds increase, as anticipated from the pressure change. The subtropical winds also increase. The pattern of change also projects on our 20C HLM, but with a coefficient (Table 3) smaller than that required to match the winds at 59°S (the LLM node), which is 1.19. Using this coefficient, and adding 1×LLM, produces the curve shown. This again matches the actual change to 45°S. It is quite different further north, where the change is more like –1×LLM (the overall projection for LLM is small, Table 3). Consistent with the Mk2 results, the projection of EOF1 for both SLP and U diminishes slowly over 22C (Table 3). The trends in EOF2 for both are also negative.

The HLM does appear to be useful in interpreting the change at high latitudes. Ring and Plumb (2007) find that the eddy feedback mechanism allows a forced change to preferentially project on HLM in a simple dynamical model. There are also several indications that the pattern of oceanic warming promotes the HLM. The SST anomalies are much larger that those in Fig. 14a, and do not die away, of course. This could act as a further long-term 'feedback' to the mode. The seasonal variation in SLP does shift with latitude along with T_s. Further, as argued by Cai et al. (2003), the HLM trend in 22C corresponds to some reversal of the Southern Ocean retardation in warming. However, the SST pattern is also a product of oceanic heat uptake and dynamics, so that it need not be due to the HLM itself.

The position of LLM as a useful mode is however poorly supported by these climate change results. The LLM may reflect some of the midlatitude response to the surface warming. However, the low-latitude wind change seems due to another mechanism, not directly related to annular variability. Increased tropical latent heating is a likely driver, as suggested by results from Jeff Yin (personal communication), see also Son and Lee (2005).

Finally, we should consider whether the annular variability, itself, within 22C differs from that in 20C. In fact, the HLM and LLM EOFs calculated from the U anomalies are almost identical to those in Fig. 3. There is merely a shift southward of about 1°, in the peaks and nodes of both, which corresponds well to that in the main jet. Further examination of the monthly indices and relationships has yielded nothing that need be added here.

8. Should the HLM and LLM be regarded as 'annular modes'?

The first EOF of zonal wind in the simulation of the SH by the Mk3 climate model, the high latitude mode, is evidently an annular mode, in a simple, statistical sense. Comparing

with previous results from Mk2, it is clear that the model upgrade has not changed the basic character of the HLM or the physical mechanisms contributing to its evolution. The topics considered here in more depth show that seasonal variation in the amplitude and persistence of the HLM in Mk3 can be qualitatively related to variation in eddy forcing and feedback and in the damping of anomalies by surface friction regulated through the model boundary layer. Relationships between EOFs within sectors point to some dynamical annularity for the HLM, particularly on timescales of two weeks or more.

This paper extends the analysis to the second EOF, a low latitude mode that can be as large as HLM in the inhabited latitudes of the SH. The structure of the LLM is again a dipole in wind representing low-latitude variance in the zonal jet. In southern winter, especially, when the jet is stronger, the behavior of the simulated LLM has much in common with HLM. However, LLM exhibits little positive eddy feedback overall, and weaker persistence, especially in sectors.

With regard to annularity, spherical geometry seems to favor the wind mode nearest the pole. By geostrophy, sea level pressure is lower towards the pole when the southern lobe in wind strengthens within a sector. For the HLM this anomaly tends to extend throughout the adjacent polar region. The resulting pressure gradients can then relate to winds in the other sectors. This effect is apparently very much weaker for the LLM.

The HLM, particularly, influences the ocean temperatures of the model, and there is a small boost to the long-term variability of the mode, relative to an atmosphere-only model. In Mk3 neither mode appears to be strongly influenced by the crude model stratosphere. Nevetheless, the Mk3 does match well the structure of the modes in the ERA40 reanalyses. Given this, and the spatial detail now simulated, the impact of the modes on regional precipitation and temperature in Mk3, to be presented elsewhere, will be of considerable interest.

In the simulation of climate change by Mk3, neither mode of variability is significantly altered in structure. However, the mean change in high latitude wind and pressure projects strongly on the HLM and also on the closely related mode in zonal mean pressure. This further the supports the usefulness of the HLM in interpreting change. Small projections of change and also of ENSO on the LLM seem rather coincidental.

So how do we answer our question? Overall, there is considerable support for the HLM as being both a statistical and dynamical annular mode, particularly on the monthly and longer timescale. The eddy feedback and proximity to the South Pole both appear to contribute to this character. Even then, the HLM explains only a small fraction of regional variability in the midlatitudes. The LLM does explain a further fraction and it may have some use. However, in Mk3, at least, it does not challenge HLM's position as being the zonal wind counterpart to the customary, and only, Southern Annular Mode.

Acknowledgements

This work is in part funded through the Australian Climate Change Science Program. The author is grateful for support from Kyoto University Active Geosphere Investigations for the 21st Century COE Program (KAGI21) to attend the Chapman Conference.

References

Ambaum, M. H. P., B. J. Hoskins, and D. B. Stephenson, 2001: Arctic Oscillation or North Atlantic Oscillation? *J. Climate*, **14**, 3495–3507.

Baldwin, M. P., D. B. Stephenson, D. W. J. Thompson, T. J. Dunkerton, A. J. Charlton, and A. O'Neill, 2003: Stratospheric memory and skill of extended-range weather forecasts. *Science*, **301**, 636–640.

Cai, W., and I. G. Watterson, 2002: Modes of interannual variability of the southern hemisphere circulation simulated by the CSIRO coupled model. *J. Climate*, **15**, 1159–1174.

Cai, W., P. H. Whetton, and D. J. Karoly, 2003: The response of the Antarctic oscillation to increasing and stabilized atmospheric CO_2. *J. Clim.*, **16**, 1525–1538.

Cash, B. A., P. J. Kushner, and G. K. Vallis, 2005: Zonal asymmetries, teleconnections and annular patterns in a GCM. *J. Atmos. Sci.*, **62**, 207–219.

Codron, F., 2005: Relation between annular modes and the mean state: southern hemisphere summer. *J. Climate*, **18**, 320–330.

Codron, F., 2007: Relations between annular modes and the mean state: southern hemisphere winter. *J. Atmos. Sci.*, **64**. this issue.

Cohen, J., and K. Saito, 2002: A test for annular modes. *J. Climate*, **15**, 2537–2546.

Feldstein, S., and S. Lee, 1998: Is the atmospheric zonal index driven by an eddy feedback? *J. Atmos. Sci.*, **55**, 3077–3086.

Feldstein, S. B., 1998: An observational study of the intraseasonal poleward propagation of zonal mean flow anomalies. *J. Atmos. Sci.*, **55**, 2516–2529.

Frederiksen, J. S., and C. S. Frederiksen, 1993: Southern hemisphere storm tracks, blocking, and low-frequency anomalies in a primitive equation model. *J. Atmos. Sci.*, **50**, 3148–3163.

Gerber, E. P., and G. K. Vallis, 2005: A stochastic model for the spatial structure of annular patterns of variability and the North Atlantic oscillation. *J. Climate*, **18**, 2102–2118.

Gerber, E. P., and G. K. Vallis, 2007: Eddy–zonal flow interactions and the persistence of the zonal index. *J. Atmos. Sci.*, **64**. this issue.

Gillett, N. P., T. D. Kell, and P. D. Jones, 2006: Regional climate impacts of the southern annular mode. *Geophys. Res. Lett.*, **33**. in press.

Gong, D., and S. Wang, 1999: Definition of Antarctic oscillation index. *Geophys. Res. Lett.*, **26**, 459–462.

Gordon, H. B., L. D. Rotstayn, J. L. McGregor, M. R. Dix, E. A. Kowalczyk, S. P. O'Farrell, L. J. Waterman, A. C. Hirst, S. G. Wilson, M. A. Collier, I. G. Watterson, and T. I. Elliott, 2002: The CSIRO Mk3 climate system model. Technical Paper 60, CSIRO Division of Atmospheric Research. www.cmar.csiro.au/e-print/open/gordon_2002a.pdf.

Kållberg, P., A. Simmonds, S. Uppala, and M. Fuentes, 2004: The ERA40 archive. ERA-40 Project Series 17, ECMWF. avail. from www.ecmwf.int/publications.

Karoly, D. J., 1990: The role of transient eddies in low-frequency zonal variations in the Southern Hemisphere circulation. *Tellus A*, **42**, 41–50.

Kidson, J. W., 1988a: Indices of the southern hemisphere zonal wind. *J. Climate*, **1**, 183–194.

Kidson, J. W., 1988b: Interannual variations in the southern hemisphere circulation. *J. Climate*, **1**, 1177–1198.

Kidson, J. W., and I. G. Watterson, 1999: The structure and predictability of the high latitude mode in the CSIRO9 general circulation model. *J. Atmos. Sci.*, **56**, 3859–3873.

Lorenz, D. J., and D. L. Hartmann, 2001: Eddy-zonal flow feedback in the Southern Hemisphere. *J. Atmos. Sci.*, **58**, 3312–3327.

Miller, R. L., G. A. Schmidt, and D. T. Shindell, 2006: Forced annular variations in the 20th century Intergovernmental Panel on Climate Change Fourth Assessment Report models. *J. Geophys. Res.*, **111**. D18101, DOI 10.1029/2005JD006323.

Pook, M. J., P. C. MacIntosh, and G. A. Meyers, 2006: The synoptic decomposition of cool season rainfall in the southeastern Australian cropping region. *J. Appl. Meteor. Climate*, **45**, 1156–1170.

Reichler, T., P. J. Kushner, and L. M. Polvani, 2005: The coupled stratosphere-troposphere response to impulsive forcing from the troposphere. *J. Atmos. Sci.*, **62**, 3337–3352.

Ring, M. J., and R. A. Plumb, 2007: Forced annular mode patterns in a simple atmospheric general circulation model. *J. Atmos. Sci.*, **64**. this issue.

Robinson, W. A., 1994: Eddy feedbacks on the zonal index and eddy-zonal flow interactions induced by zonal flow transience. *J. Atmos. Sci.*, **51**, 2553–2562.

Seager, R., N. Harnik, Y. Kushnir, W. Robinson, and J. Miller, 2003: Mechanisms of hemispherically symmetric climate variability. *J. Climate*, **16**, 2960–2978.

Sen Gupta, A., and M. H. England, 2006: Coupled ocean-atmosphere-ice response to variations in the southern annular mode. *J. Climate*, **19**, 4457–4486.

Son, S.-W., and S. Lee, 2005: The response of westerly jets to thermal driving. *J. Atmos. Sci.*, **62**, 3741–3757.

Thompson, D. W. J., and J. M. Wallace, 2000: Annular modes in the extratropical circulation, Part I, Month to month variability. *J. Clim.*, **13**, 1000–1016.

Wallace, J. M., 2000: North Atlantic Oscillation/annular mode: Two paradigms-one phenomenon. *Q. J. Roy. Met. Soc.*, **126**, 791–805.

Watterson, I. G., 2000: Southern midlatitude zonal wind vacillation and its interaction with the ocean in GCM simulations. *J. Clim.*, **13**, 562–578.

Watterson, I. G., 2001: Zonal wind vacillation and its interaction with the ocean: implications for interannual variability and predictability. *J. Geophys. Res.*, **106**, 23965–23975.

Watterson, I. G., 2002: Wave-mean flow feedback and the persistence of simulated zonal flow vacillation. *J. Atmos. Sci.*, **59**, 1274–1288.

Watterson, I. G., and M. R. Dix, 2005: Effective sensitivity and heat capacity in the response of climate models to greenhouse gas and aerosol forcings. *Quart. J. Roy. Met. Soc.*, **131**, 259–280.

Watterson, I. G., and J. Syktus, 2006: The influence of air-sea interaction on the Madden-Julian Oscillation: the role of the seasonal mean state. *Clim. Dyn.* in press.

Yu, J.-Y., and D. L. Hartmann, 1993: Zonal flow vacillation and eddy forcing in a simple GCM of the atmosphere. *J. Atmos. Sci.*, **50**, 3244–3259.

List of Figures

	w	r-S1	r-S2	r-S3	r-S4
HLM					
Zon	0.92	70	78	77	68
S1	1.18		38	34	39
S2	1.36			55	32
S3	1.14				45
S4	1.11				
LLM					
Zon	0.60	57	71	66	33
S1	0.75		36	08	12
S2	1.04			31	−4
S3	1.28				−6
S4	0.90				

Table 1: Statistics of HLM and LLM modes, from monthly means and U averaged over whole zone (Zon) and four 90° sectors, S1 (0°E-90°E), S2 (90°E-180°E), and so on. Given are representative wind speed w ($\mathrm{m\,s^{-1}}$, see text), and cross-correlations $r \times 100$ with other indices. HLM is EOF1, and LLM is EOF2, except that the reverse holds for S3.

Index	Lagged Index	−1	0	1
LLM	HLM	–19	0	22
u50-1	HLM	14	53	33
u50-2	LLM	23	48	15
u50-1	Utr-1	10	47	31
u50-2	Utr-2	21	43	12
u50-1i	Utr-1	–10	0	13
u50-1i	Utr-2	5	36	9
u50-2i	Utr-2	10	0	1
u50-2i	Utr-1	9	19	11

Table 2: Correlations ($r \times 100$) between pairs of monthly indices, with the second index lagged by the month in the header. HLM and LLM refer to the U PCs. u50-1 and u50-2 are the PCs from u at ~ 50 hPa. Utr-1 and Utr-2 are the PCs from tropospheric integrated wind (to 125 hPa). u50-ni is u50-n with the component correlated to Utr-n removed.

Quantity	PC1	PC2
Change SLP	1.00	–0.44
Change U	0.70	0.06
Trend SLP	–0.25	–0.19
Trend U	–0.19	–0.39

Table 3: Projection of climate changes, in SLP and U, on the 20C modes determined from the same quantity, in terms of the mode index (SD=1). Change represents the mean change (22C–20C). Trend is the trend per 100 y, during 22C.

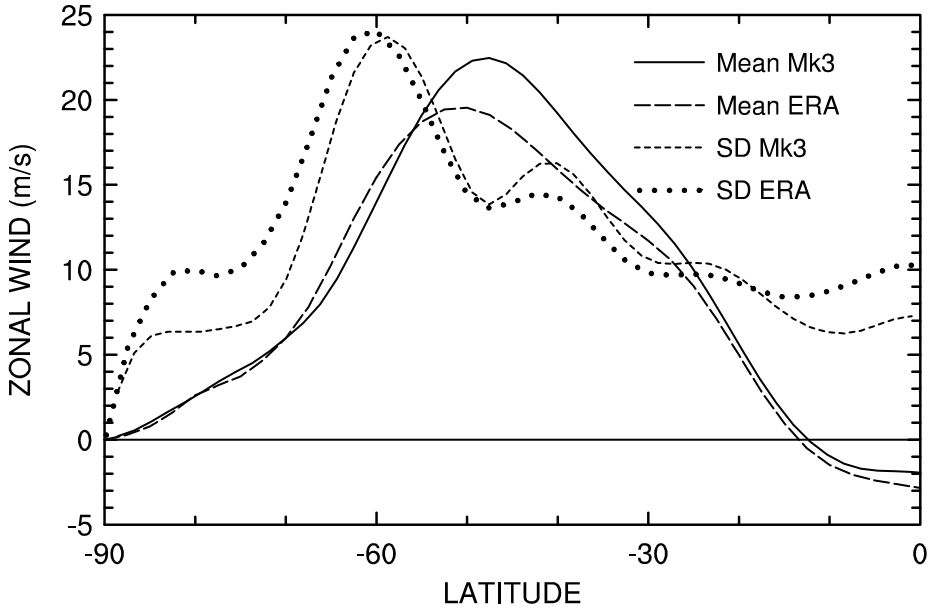

Figure 1: Statistics of the vertically integrated zonal mean zonal wind (U) from Mk3 and ERA. Shown are annual mean U, together with standard deviation ($\times 10$, to allow a single scale) of the monthly mean U (see key).

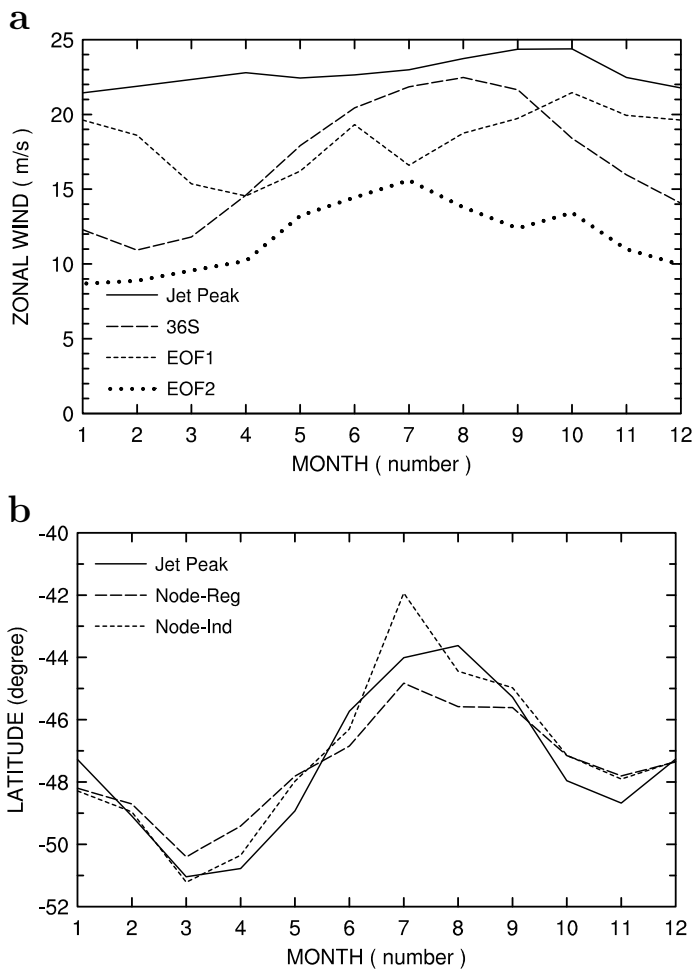

Figure 2: Annual cycle of the structure in U and modes from Mk3, from monthly values: (a) speed of midlatitude jet peak, speed at 36°S, and representative wind speed ($w \times 20$) of EOF1 and EOF2; (b) latitude of jet peak, and latitude of node of EOF1 pattern obtained from regression (Reg) and of EOF1 from analysis of each individual month (Ind).

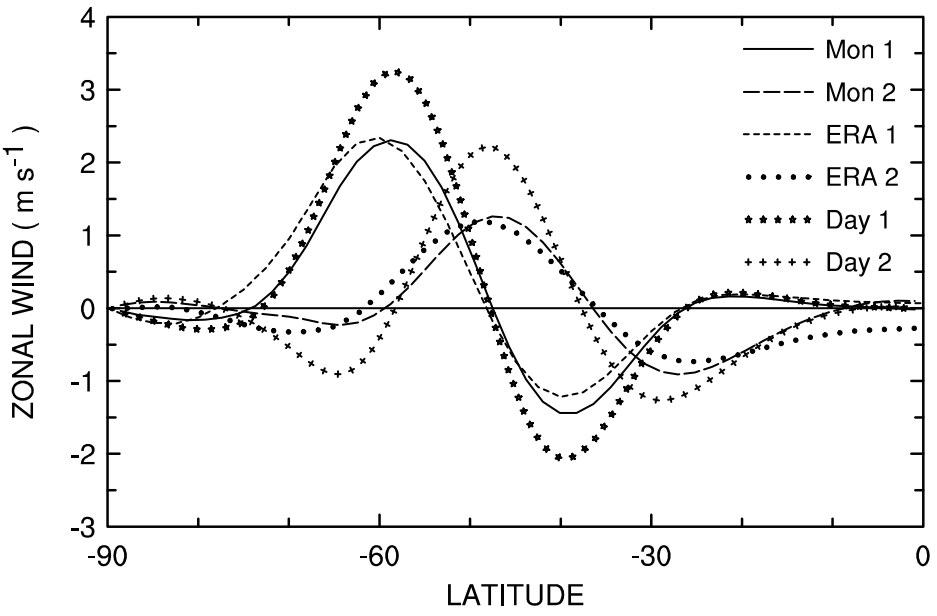

Figure 3: EOF1 and EOF2 from analysis of U. 'Mon' refers to monthly means from Mk3, and 'ERA' to monthly means from ERA. 'Day' refers to analysis of daily (6-hourly) data from Mk3.

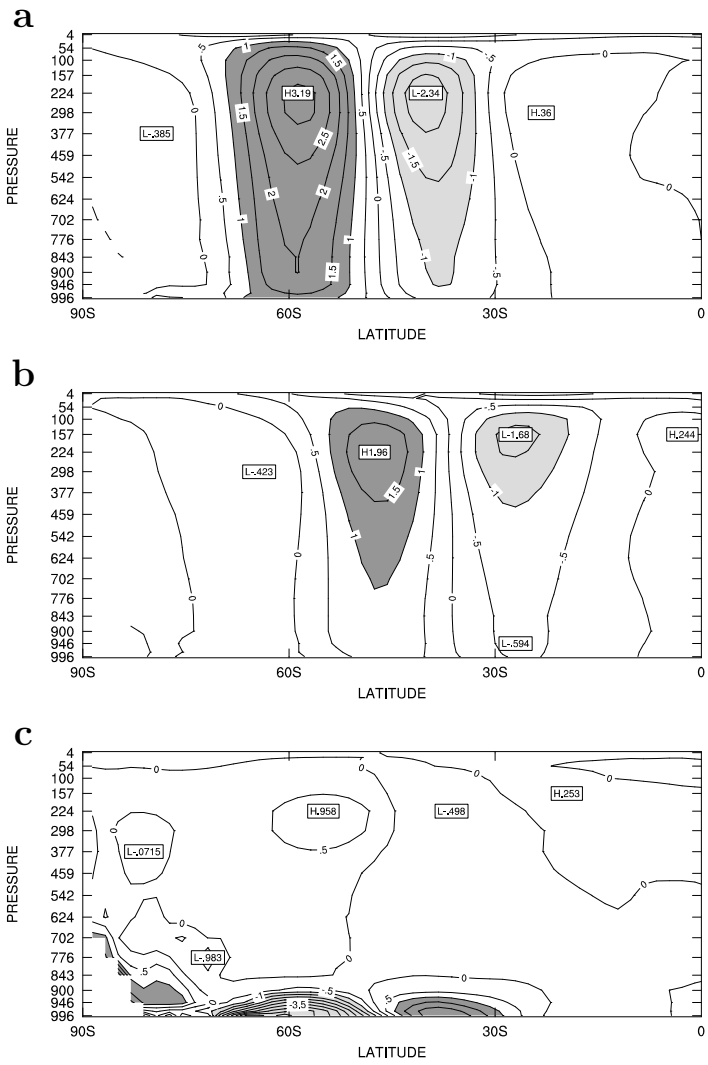

Figure 4: Structure of zonal mean wind anomalies ($\mathrm{m\,s^{-1}}$) associated with the modes from Mk3, from the regression coefficient between monthly means: for u (a) HLM and (b) LLM; for v (c) $\times 10$ HLM. Contour interval 0.5 $\mathrm{m\,s^{-1}}$, with magnitudes over 1 shaded. Pressure levels of the data are indicated (except for 22 and 978 hPa).

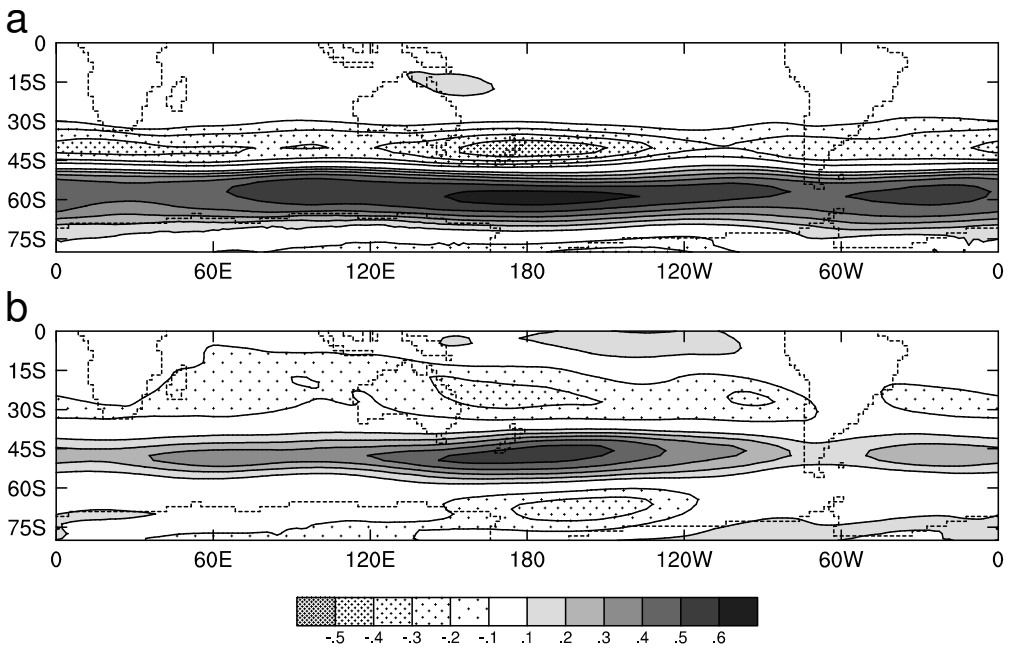

Figure 5: Correlation r between monthly indices and U at grid points: (a) HLM, and (b) LLM. The model coastline is shown.

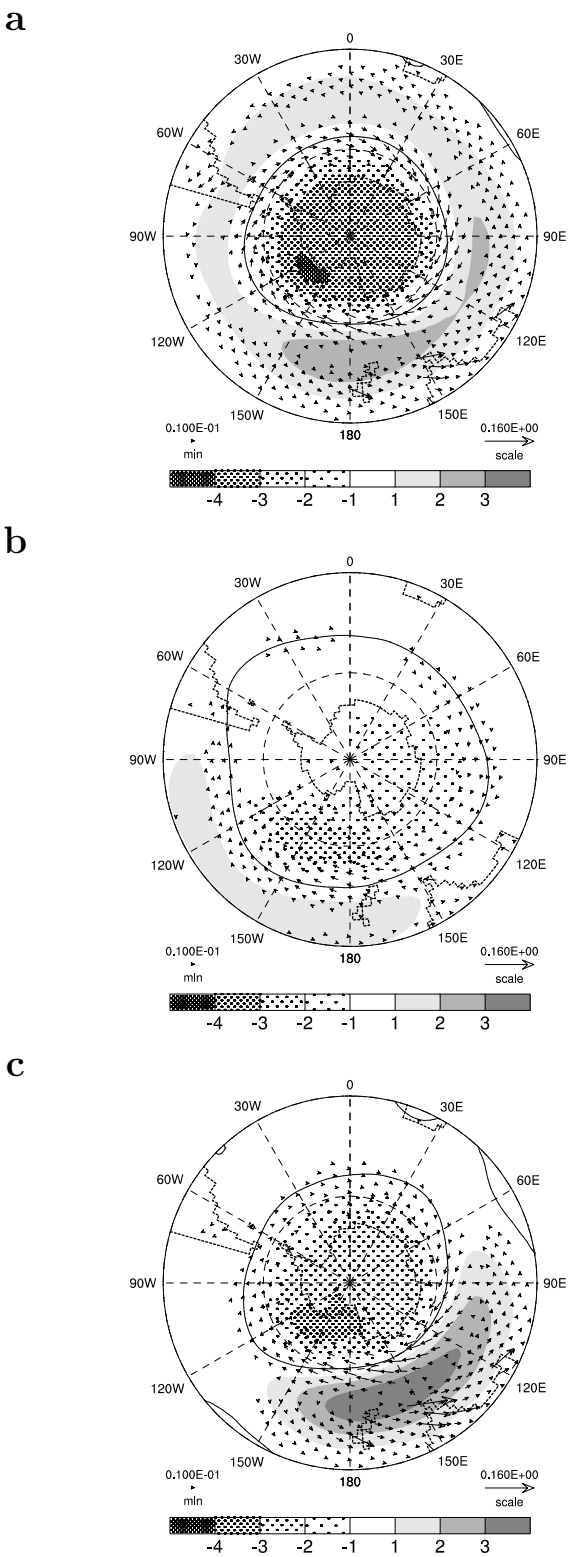

Figure 6: Regression coefficients between monthly indices and surface quantities at grid points: (a) HLM, (b) LLM, (c) Australian sector (S2) HLM. Shown as shading (and zero contour), sea level pressure (hPa); and as vectors, surface stress (N m^{-2}).

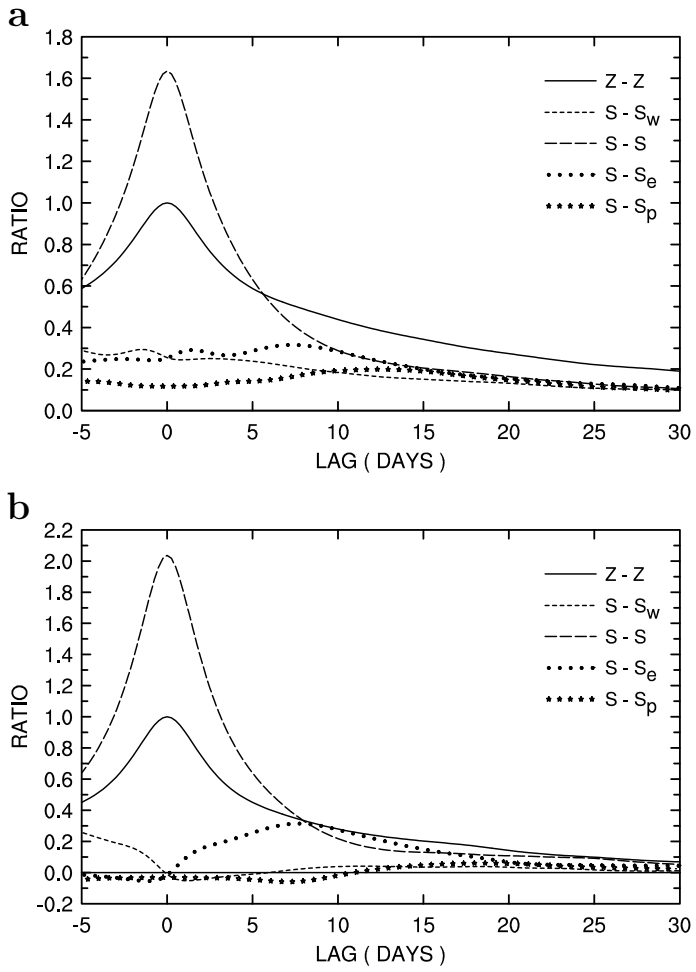

Figure 7: Regression coefficients between pairs of daily indices (as in the key, the second index being lagged) associated with: (a) HLM, and (b) LLM. Z refers to the zonal-mean index, S to the sector indices. Subscripts on the second index mean the sector to the east ('e'), or the west ('w'), or across the pole ('p'). The values are averaged over the four sectors for the first index (including a weighting by wind speed w). To give a representative magnitude relative to the zonal case, the second index is multiplied by the ratio of its w to the zonal w, hence the axis label.

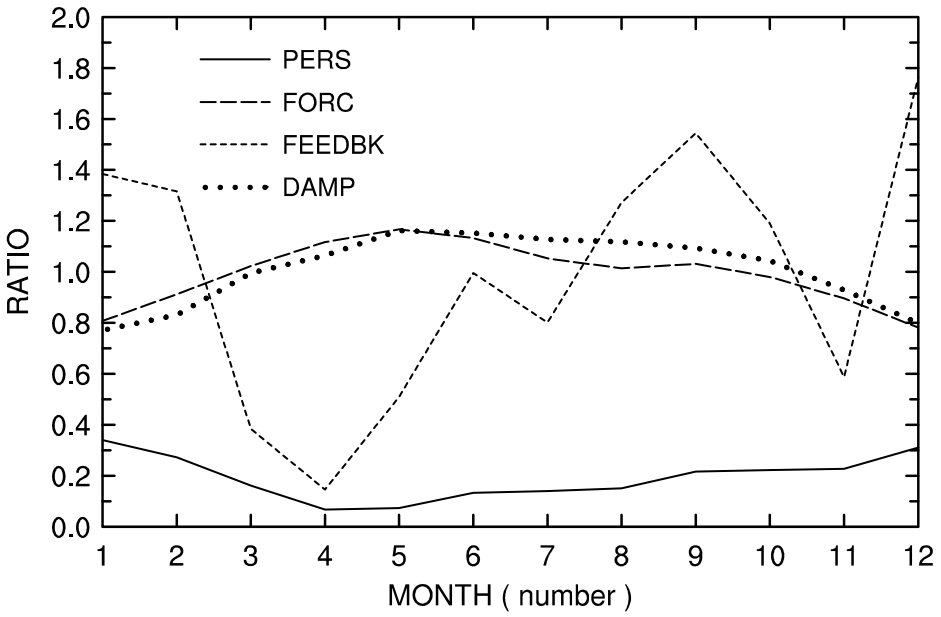

Figure 8: Annual cycle of statistics associated with the evolution of HLM. PERS is the one-month autocorrelation of the daily index (with each month), averaged from values at lags +30 d and −30 d. FORC is the SD of the daily F_E series, partitioned by month. FEEDBK is the average of the F_E regression b, over lags +10 d to +30 d. DAMP is the b for the monthly average of term D, relative to the monthly HLM. The last three are shown as a ratio with the value taken from an annual analysis.

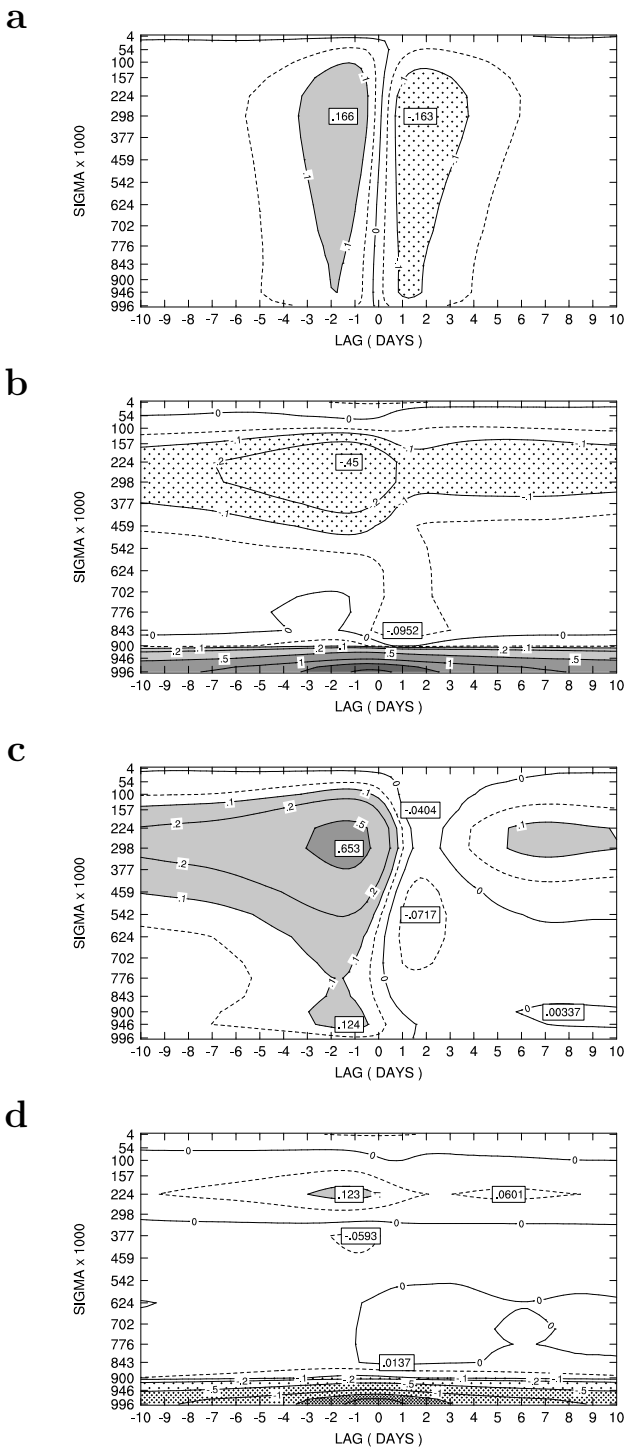

Figure 9: Regression coefficient between the HLM daily index and momentum budget quantities at sigma levels, over lags -10 d to 10 d: (a) u_t, (b) fv, (c) F_E, and (d) D. Contour interval 0.5 (in unit per day), together with ± 0.05 (dashed), 0.1 and 0.2. Shading for magnitudes over 0.1.

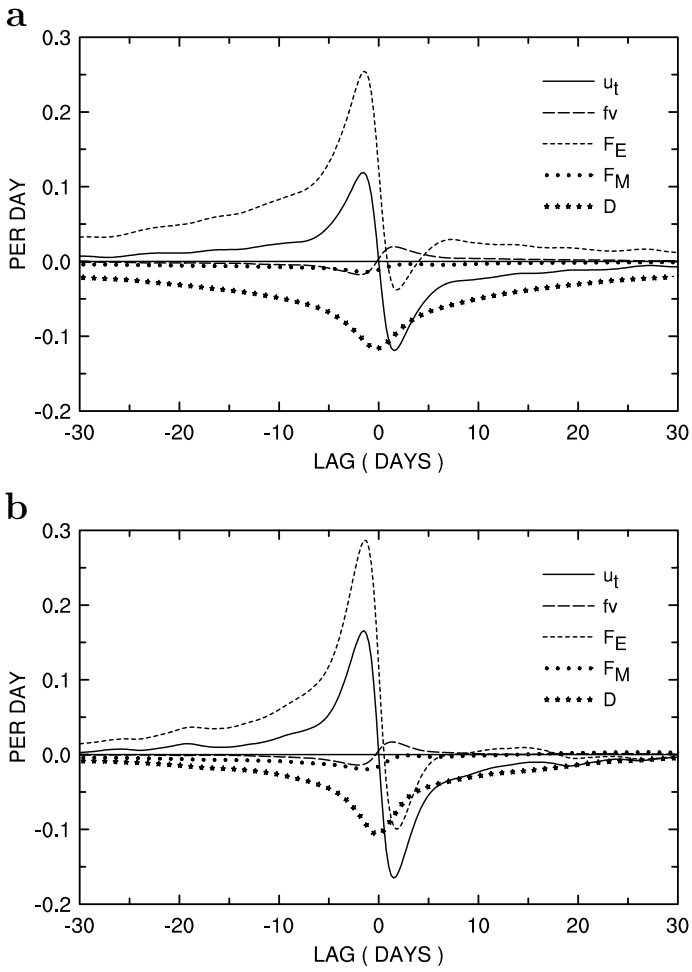

Figure 10: Regression coefficient between the daily indices and momentum budget quantities vertically integrated, over lags −10 d to 10 d: (a) HLM, and (b) LLM.

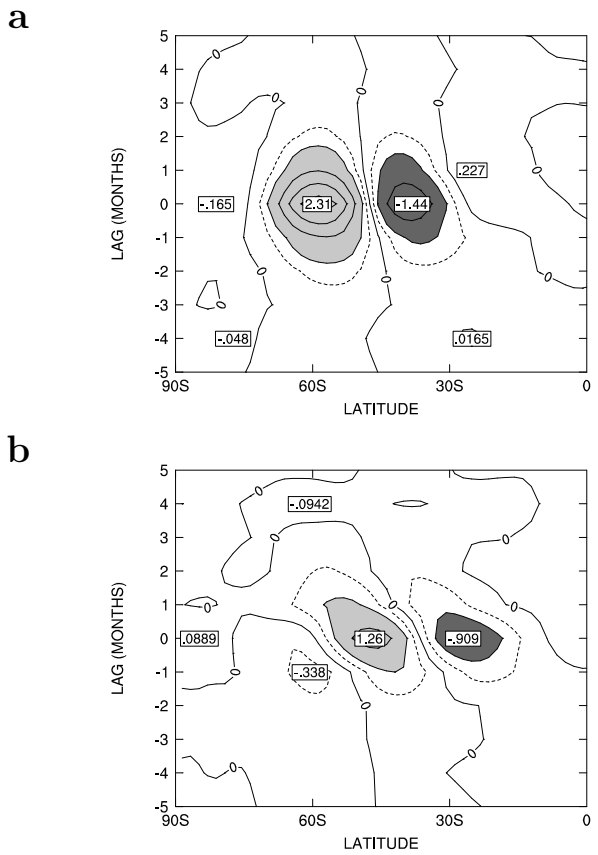

Figure 11: Regression coefficient between the monthly indices and (zonal mean) U, lagged by from –5 to +5 months: (a) HLM, and (b) LLM. Contour interval 0.5 $\mathrm{m\,s^{-1}}$, together with ± 0.25 (dashed).

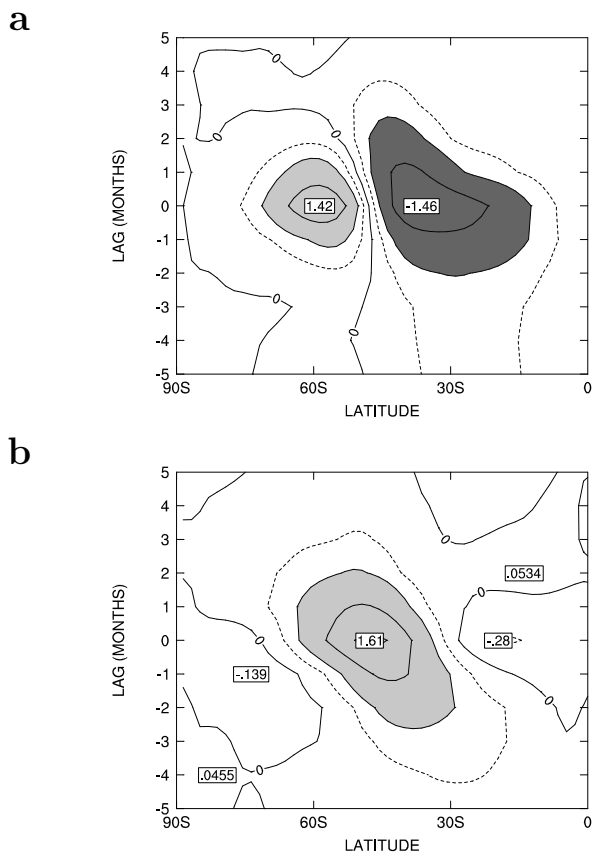

Figure 12: Regression coefficient between the indices (u50-n) of zonal mean zonal wind at 54 hPa and the wind itself lagged by from –5 to +5 months: (a) EOF1, and (b) EOF2. Contour interval 0.5 $\mathrm{m\,s^{-1}}$, together with ± 0.25 (dashed).

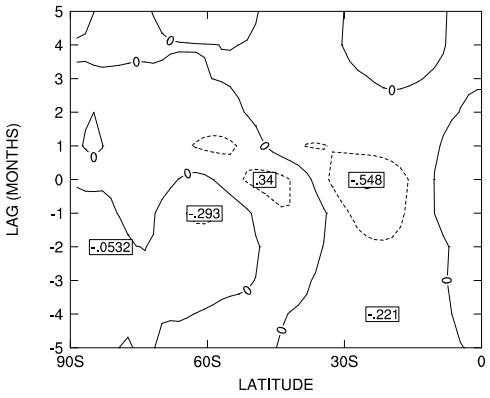

Figure 13: Regression coefficient between the u50-1i index (SD 0.88) and u vertically averaged over the troposphere. Contour interval 0.5 $\mathrm{m\,s^{-1}}$, together with ± 0.25 (dashed).

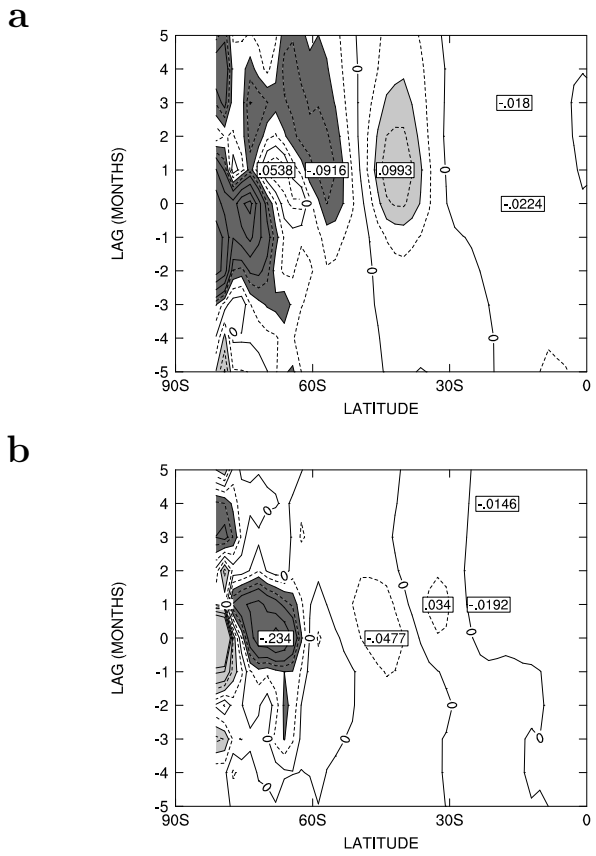

Figure 14: Regression coefficient between the monthly index and zonal mean ocean surface temperature (including sea ice), lagged by from –5 to +5 months : (a) HLM, and (b) LLM. Contour interval 0.05 K, together with ±0.025, and ±0.075 (dashed). Magnitudes above 0.05 K shaded.

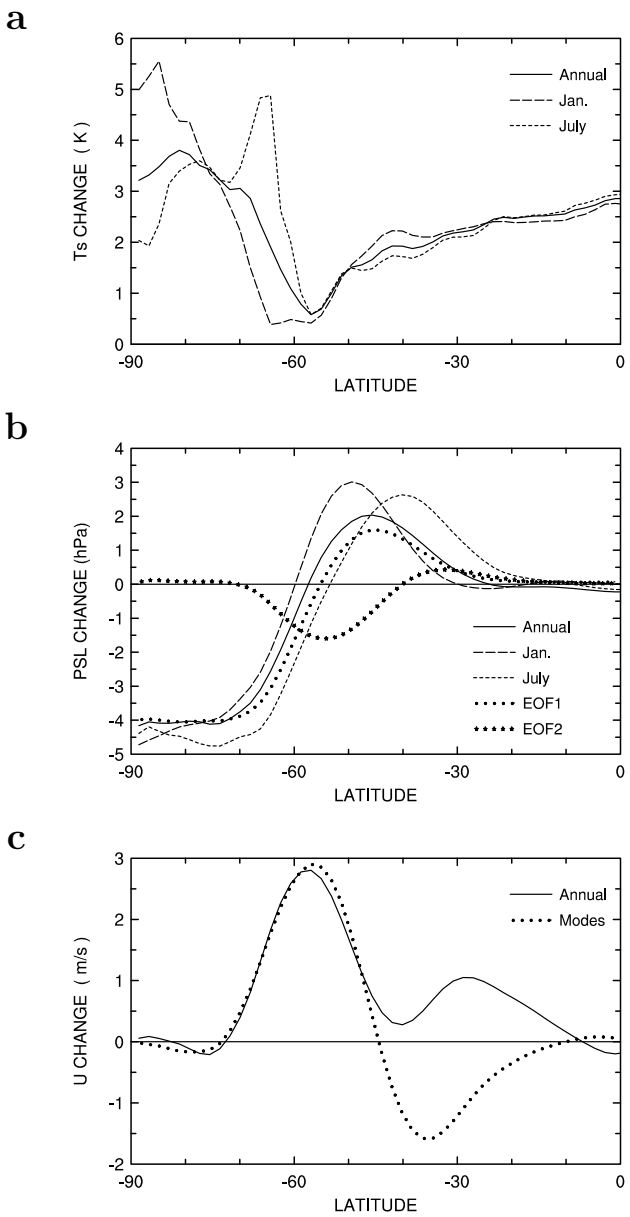

Figure 15: Change from 20C climate to 22C climate, in zonal means over SH, compared to Modes: (a) T_s, (b) SLP, and (c) U. Shown are the Annual mean changes, together with January and July results. For SLP, the EOF1 and EOF2 are shown. For U, the sum of 1.19×HLM and LLM is shown as 'Modes' (see text).